NANO LETTERS

2006
Vol. 6, No. 9
1875−1879

Dynamics of Polymorphic Nanostructures: From Growth to Collapse

F. Carlier,[†] S. Benrezzak,[†] Ph. Cahuzac,[†] N. Kebaïli,[†] A. Masson,[†] A. K. Srivastava,[‡,§] C. Colliex,[‡] and C. Bréchignac*[,†]

Laboratoire Aimé Cotton CNRS, Bât. 505, Université Paris-Sud, 91405 Orsay Cedex, France, and Laboratoire de Physique des Solides (UMR CNRS 8502), Bât. 510, Université Paris-Sud, 91405 Orsay Cedex, France

Received April 6, 2006; Revised Manuscript Received June 28, 2006

ABSTRACT

The deposition of preformed clusters on surfaces offers new possibilities to build complex artificial nanostructures, the shape of which depends on the cluster size. We describe routes for generating unusual polymorphic nanoislands, which constitute unique platforms for exploring instabilities. As coverage increases, the constraints accumulated in such nanostructures induce spectacular flattening collapse processes, which are not observed when the constraints are imposed by the substrate.

The growth processes of nanostructures on surfaces are well understood. However, the relaxation mechanisms after growth have not been thoroughly studied. Moreover they may depend on the growth processes by themselves. When the epitaxial growth on a substrate is studied, using atom per atom deposition, the lattice misfit between the substrate and the overlayers is responsible for strain-driven transitions in order to offer the overlayers the possibility of recovering a relaxed lattice parameter. Generally, a two-dimensional (2D) to three-dimensional (3D) transformation gives rise to islanding, which has been recognized as essential for growing nanostructures.[1,2]

The reverse situation, where the elastic strain is accumulated in nanostructures in weak interaction with a substrate, has not been studied up to now. One of the reasons for the lack of such an investigation may be due to the scarcity of growth processes generating at will artificial nanoobjects with a large degree of shape complexity, which could exhibit intrinsic relaxation mechanisms. To generate such systems, we construct nanoislands from the controlled deposition of preformed clusters, which by themselves constitute 3D building blocks, i.e., the "cluster route" differs from the standard "atomic route", involved in molecular beam epitaxy. It results into a family of metastable structures at the nanoscale,[3−7] which constitute a platform for exploring instability driven changes at this scale.[8,9] Evidence of an unusual morphological transition, as a spectacular collapse from compact structures toward flattened ones, i.e., of 3D to 2D type transition, is shown. For sake of clarity, our paper successively describes and discusses: (i) the growth of different morphologies as a function of the cluster size $\langle n \rangle$; (ii) the generation of polymorphic shapes as the output of a sequence of deposits with different $\langle n \rangle$; (iii) the occurrence of cooperative shape transformations taking place as coverage increases, such as the observed spreading processes, and showing similarities with catastrophic events.[10]

A neutral antimony cluster beam, produced by a gas-aggregation cluster source,[11] is deposited at low impact energy (0.05 eV/atom), on a room-temperature cleaved graphite surface maintained under high vacuum (10^{-9} Torr). The neutral cluster size distribution is measured by a time-of-flight mass spectrometer. It exhibits the well-known prevailing Sb_{4p} masses, i.e., a higher abundance of clusters made of a multiple of Sb_4 units, which gradually fades out as the total mass of the clusters increases. The average cluster size $\langle n \rangle$ is tuned by changing the source conditions (inert gas pressures and oven temperature). A quartz microbalance measures the flux of the incident clusters (of the order of 10^{10} clusters/(cm^2 s), with deposition times between 1 and 10 min). Since the per-atom kinetic energy of the incident clusters is very low compared with their binding energy (1.5 eV/atom), the clusters migrate on the surface as a whole and grow into islands.[3,4] The prepared samples are either transferred into high vacuum and imaged with a noncontact atomic force microscope (AFM) or transferred in air and imaged in a scanning transmission electron microscope (STEM). The similarity between the images obtained in both cases shows that the transfer in air does not affect the island

[†] Laboratoire Aimé Cotton CNRS, Bât.505, Université Paris-Sud.
[‡] Laboratoire de Physique des Solides (UMR CNRS 8502), Bât. 510, Université Paris-Sud.
[§] Permanent address: Division of Materials Characterization, National Physical Laboratory, Dr. K. S. Krishnan Road, New Delhi 110 012, India.

10.1021/nl060781n CCC: $33.50
Published on Web 07/19/2006

morphologies. These two imaging tools allow a complete topological mapping of the samples. The AFM measurements lead to absolute values of the elevation maps with a high accuracy, while the lateral dimensions suffer from tip convolution effects. On the other hand, STEM imaging performed in the high angle annular dark field (HAADF) mode provides images with potential sub-nanometer spatial resolution but can only map the local thickness semiquantitatively because references are required.

In the first set of experiments, we have characterized the morphological parameters of islands grown by slow deposition of preformed clusters on surfaces, as a function of cluster size. Previous studies[4] have shown that the mobility of clusters as a whole and their coalescence rate, both factors depending on the number of atoms they are made of, interplay to govern the final shape of the synthesized nanoobjects. Increasing cluster size leads to island structures that evolve from compact to seaweed and then to fractal morphology (see images exhibiting these typical morphologies grown from the deposition of Sb_{88} and Sb_{300} in the Supporting Information). Ramified island shapes are characterized by four parameters: the extended size L that is the diameter of the smallest circle enclosing the whole island, the typical branch width l, the fractal dimension D_f,[12] and the height of the arms h. In our experimental conditions L varies between 500 nm and 1 μm. We verify that both the height h and the width l of the arms are nearly constant along the direction of branching. They are only governed by the cluster size.[4] For $\langle n \rangle = 300$, $l = 8$ nm, and $h = 4$ nm. The fractal dimension D_f, which describes the compactness of the structure, is obtained from the scaling relation between the mass M and the radius of gyration r_g of islands, $M \sim r_g^{D_f}$.[11] The two situations with Sb_{88} and Sb_{300} incident clusters correspond to two families of ramified objects, respectively, with a seaweed structure characterized by a small number of broad arms and a fractal dimension $D_f = 1.8$, and with a fractal structure characterized by a larger number of thinner arms and a fractal dimension $D_f = 1.65$.

As the island morphology can be controlled by changing the cluster size, polymorphic objects can therefore be synthesized, in a given experiment, by sequential depositions of clusters with two different average sizes. In Figure 1a, we have first deposited antimony clusters of $\langle n \rangle = 88$, then those of $\langle n \rangle = 300$ by modifying the cluster source operating conditions. In Figure 1b, the reversed deposition sequence was applied. We initially ensure that the coverage of the first deposit is higher than that of the second one, so that the first deposit dominates the resultant island shape. Dimorphic islands exhibiting distinct structures are then obtained. In the first case of small-then-large cluster deposition, the island is made of a thick central part with a seaweed-like shape and of thinner outer branches. On the contrary, in large-then-small cluster deposition, the islands have centers with ramified thin branches, and they terminate with compact structures.

To estimate the role played by the deposition of different cluster sizes on the final island shape, we have performed Monte Carlo simulations of the island formation from

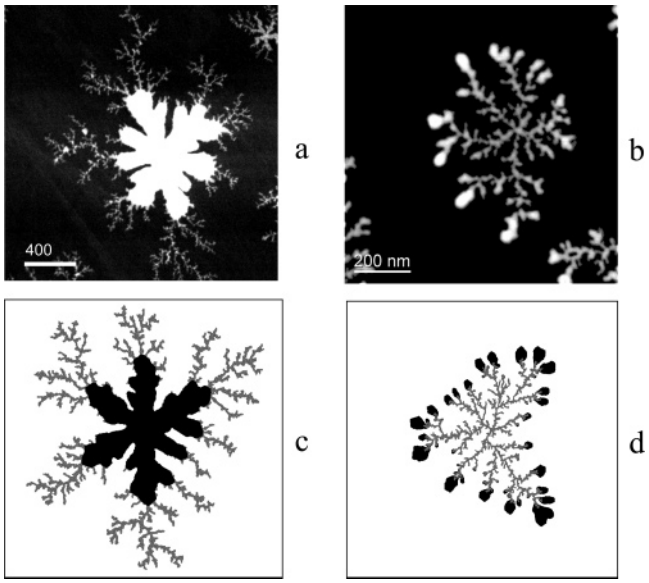

Figure 1. STEM images of dimorphic shapes grown from sequential depositions of clusters of two different sizes on the same surface: (a) the deposition of $\langle n \rangle = 88$ was followed by the deposition of $\langle n \rangle = 300$. $\theta = 1.0$ ML and $\theta = 0.7$ ML for $\langle n \rangle = 88$ and 300, respectively. (b) The deposition of $\langle n \rangle = 300$ was followed by the deposition of $\langle n \rangle = 88$. $\theta = 0.5$ ML for $\langle n \rangle = 300$, and $\theta = 0.3$ ML. Different sizes of incident clusters are obtained by changing the oven temperature and the pressure of the carrier gas. (c) and (d) show simulations of the island formation on a 2D hexagonal lattice, with clusters of different sizes (courtesy of B. Yoon, presently at Georgia Institute of Technology, Atlanta, USA). They use a Brownian motion description for the cluster motion on the lattice with hopping length equal to the hexagonal lattice parameter. The clusters are created at the edges of the surface and move until they reach the island. The cluster coalescence process is included in the simulations by allowing the atoms of the aggregating cluster to hop along the island edges. The hopping rate is of the Arrhenius form, given by $p(m) = p_0 \exp(-mE_b/k_BT)$, where m is the number of broken bonds after the hopping, E_b is the diatomic bonding energy, and p_0 is a prefactor that is of the order of the typical atomic vibration frequency ν_{atom}. The evaporation of the atom is not allowed. The central part for (c) is generated from 20 000 clusters made of 7 atoms and the outer structure from 3000 clusters made of 37 atoms. For (d) the reverse procedure with respect to (a) has been performed. The numbers of clusters involved in the simulation are 4000 for 37-atom clusters and 15 000 for 7-atom clusters. We have introduced the following values as the simulation parameters: $E_b/k_BT = 10.0$ and $p_0 = 10^{12}$ s^{-1} in the equation in ref 15, and $\Delta t = 5 \times 10^{-3}$ s.

preformed clusters on a 2D hexagonal lattice for the two reverse sequences with different $\langle n \rangle$. The simulation results in parts c and d of Figure 1 for the two experimental sequences show an evolution of the branch width that appears as a juxtaposition of the two growth models.

In the case of small-then-large cluster deposition, the thicker seaweed particle grown from the small cluster deposition (typically between 1 and 2 monolayers (ML)) plays the same role as a large defect for the growth of the thin dendritic arms generated by the large cluster deposition. As no steric obstacle prevents the arrival and aggregation of further incident clusters, there is no difficulty for growing nanodendrites out of a thicker compact particle. The branch profile shows both constant height and width along the branching direction from the compact high central part to

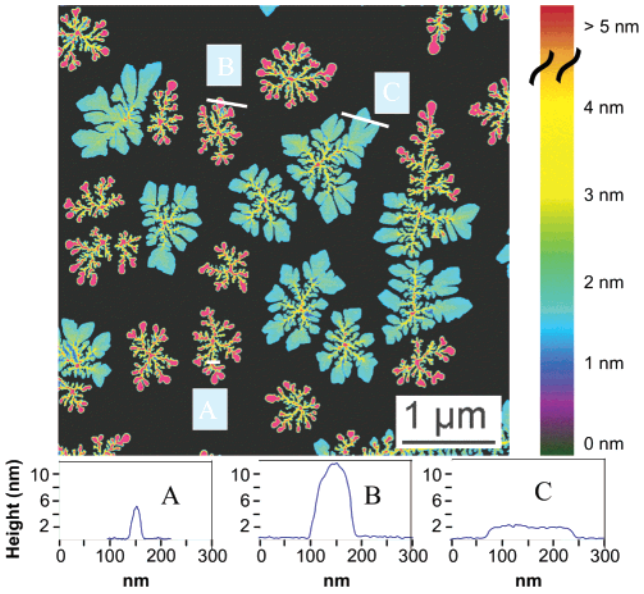

Figure 2. Composite nanostructures exhibiting polymorphism, obtained from two consecutive depositions of Sb clusters: 1 ML of Sb_{300} (the yellow fractal center) then 6 ML of Sb_{88} (endings) on graphite substrate. The endings (red) are compact up to a critical coverage (>2 ML) where some islands exhibit a flattening transition accompanied with crystallization (green). The color scales green, yellow, and red correspond to increasing thicknesses from 2 to 15 nm. Cross sections of different parts of islands, corresponding to the white lines A, B, and C, show their heights (lower traces).

its extremity, in agreement with a juxtaposition of the growth models, see parts a and c of Figure 1. The final morphology of the island remains the same when increasing the coverage of the second deposit.

On the contrary, the deposition of large-then-small clusters shows that the initial fractal island obtained after the deposition of Sb_{300} is perturbed by the following deposit of Sb_{88}, which slightly increases the width of the arms (see Figure 1b). It suggests that the deposited Sb_{88} can penetrate toward the center of the island. Moreover, the fractal endings act as anchors for the Sb_{88}, and the deposition of large-then-small clusters closes the island structure. How far can the endings grow?

Superimposed to an initial 1 ML coverage of Sb_{300}, increasing the coverage of the second deposit Sb_{88} up to 9 ML shows evidence of a spectacular collapse transition island-by-island (see Figure 2), revealed by the coexistence of two types of island morphologies in the same sample. They exhibit endings either with thick droplike structures or with thin flat faceted shapes, the respective heights of which lie in the ranges of 10−15 nm and 2−3 nm (see typical intensity profiles reported in Figure 2 bottom). For comparison, the height of the branches in the ramified core initially grown from Sb_{300} is of the order of 5 nm. We can deduce from this observation that during the growth process, the endings of the fractal objects built from the arrival of Sb_{88} clusters become unstable and, for a given accumulated mass, spread over the free graphite surface. The polygonal shape of the flat endings, observed by AFM under vacuum, shows that they correspond to crystalline structure.

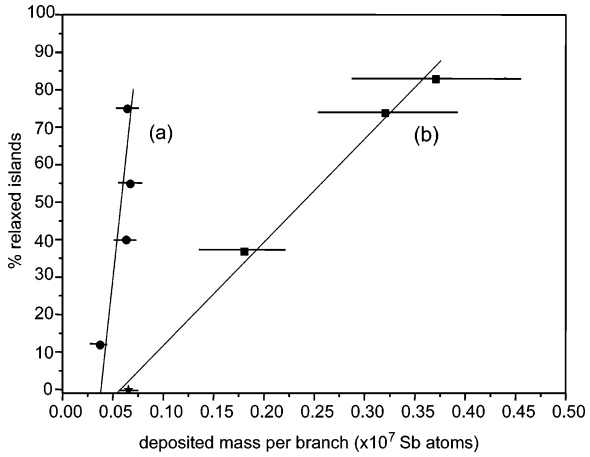

Figure 3. Plots of the percentage of islands exhibiting flattened endings, measured over wide areas for two different sequences of deposits, (a) corresponding to $\langle n \rangle = 300$ followed by $\langle n \rangle = 88$, (b) $\langle n \rangle = 300$ followed by $\langle n \rangle = 110$, as a function of the coverage in the second type of deposited clusters. This coverage is expressed in terms of total numbers of Sb atoms per branch, to emphasize the relation between the transition rate and the mass accumulated in the branches.

To get insight into the flattening transition, we have analyzed in detail both island morphologies, having undergone shape transition or not, for different specimens at different coverage.

(i) When considering an ensemble of islands lying over large specimen areas, one notices that all branches pertaining to a given island have similar endings: either all of 3D type with a dense hemispherical cap or all with a flat polygonal foot. This argument pleads in favor of a cooperative transition at the scale of the island, rather than a local one at different arm endings.

(ii) As the coverage increases, the number of islands with flat endings rises, showing evidence of a shape transition as the deposited mass increases. Different deposits corresponding to increased coverage have been examined, to relate the probability of flattening transition to the local mass estimated in the island endings. Figure 3 shows the results of these measurements for a series of deposits of two different cluster sizes: (a) $\langle n \rangle = 300$ followed by $\langle n \rangle = 88$; (b) $\langle n \rangle = 300$ followed by $\langle n \rangle = 110$. In both cases, rather linear increases are observed up to nearly complete transitions to 2D flattened morphologies. The slopes are however quite dependent on the cluster size of the second deposit. For smaller cluster deposits, the transition rate increases more efficiently than for the larger ones. In both cases, a critical mass corresponding to the onset of the straight lines is necessary to initiate the transitions. Nevertheless, it is not possible to determine, within the accuracy of the experiments, whether the critical mass depends on the cluster size. These critical masses are estimated to be of the order of a few 10^5 atoms in the individual endings.

(iii) We now focus on the shape of the radial branches and on their relative height (h) and width (l), as a function of the position x along the branch (Figure 4). We consider that the individual arm profiles in different islands are representative snapshots of their shape evolution before and

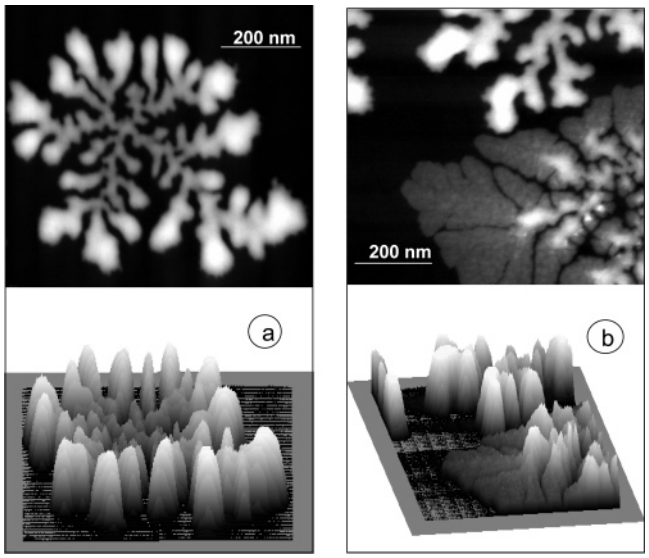

Figure 4. HAADF STEM projection and 3D views of typical island morphologies "before" (a) and "after" (b) the 3D to 2D flattening shape transition: (a) corral-type morphology of an island exhibiting a regular increase of the width and height of radial branches from center to outer areas; (b) detailed view of endings belonging to neighboring islands having suffered or not from the collapse process; it clearly reveals repulsive effects between branches of different islands

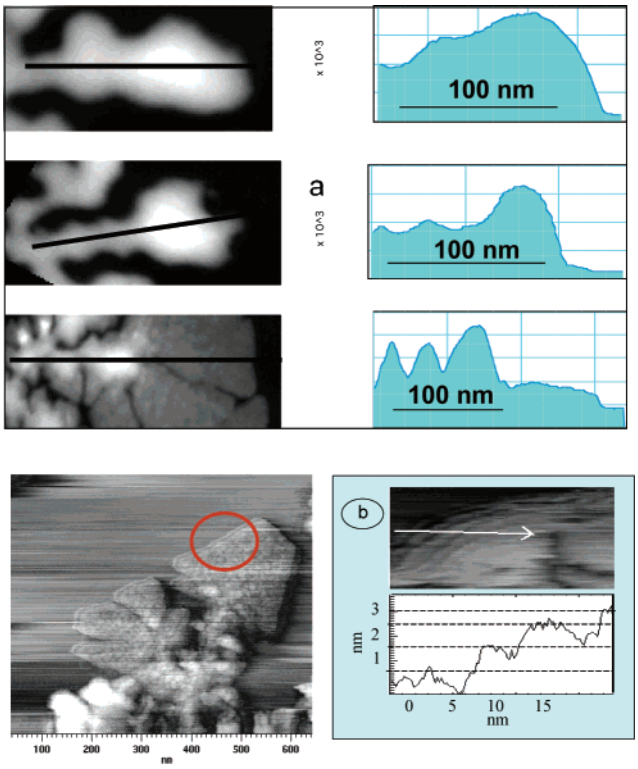

Figure 5. (a) Selection of HAADF STEM top views and thickness profiles along individual island arms "before" and "after" the flattening shape transition. (b) STM image of a flattened extremity and detailed analysis of the rim revealing its layer-by-layer nature.

after the flattening transition. For those islands which have not yet reached the flattening transition, both branch width l (Figure 4a upper image) and height h (Figure 4a lower image) regularly increase from the center zone toward the outer extremities. The global shape of the island exhibits a corral-type morphology with an outer rim made of thicker parts nearly in contact and of a shallower central area. Interestingly, for increased deposits, fluctuations in width and height along the arms become clearly visible, with increasing amplitudes and quasi-periodicity, until the collapse occurs (Figure 5a).

(iv) Considering the islands that have spread over the underlying surface, we do not find any evidence of an epitaxial relation with the graphite, as it could be deduced from orientation similarities between flat ending contours and the substrate (or diffraction patterns or moiré fringe systems). The layered morphology revealed by STM along the rims (Figure 5b) confirms the existence of a crystalline structure associated with the collapse of the island endings. In accordance with the results of Bernhardt et al.,[13] the thickness of the individual layers is larger than the interlayer spacing in the α-Sb bulk phase. These authors have proposed structural models based on the arrangement of Sb_4 tetrahedrons, leading to new structures with variable spacing distances. Our own observation of a layer-by-layer spreading in the final stage of the collapse therefore constitutes a signature of a Sb_4 memory effect, the Sb_4 species being the most abundant ones in the free cluster beam. Furthermore, the images reveal clear repulsion effects between facing endings on different islands (such as shown in Figure 4b), either between flat ones or between endings with different shapes (compact and flat). This behavior suggests the influence of strain and elastic deformation ("rumpling") induced on the substrate surface by the presence of the growing islands.

If the observations for small-then-large cluster deposition are straightforwardly understandable, the reversed situation is more complex. The first deposit ($n = 300$) produces a central fractal part, that is an open morphology into which the more mobile ($n = 88$) clusters of the second deposit can diffuse. During this second stage, the Sb_{88} clusters, which favor aggregation into compact 3D shapes, are forced to grow on the fractal arms that act as cylindrical 1D seeds. This results in an accumulation of strain energy, as the coverage increases. In parallel, local fluctuations in the kinetics of the growth mechanism are induced by the complexity of the diffusion paths of the arriving clusters at different positions along the fractal island contours. Instabilities are then likely to occur, leading to the observed quasi-periodical structures along the arms with increasing strain as the coverage increases.

To release the strain energy (proportional to the mass) stored within the volume of the growing branch and its extremity, the present study shows evidence of a global collapse, accompanied by a crystallization process. Such a phenomenon occurs when the gain in strain energy release is larger than the cost in increased surface energy. Before transition, the competition between kinetics and thermodynamics results in compact endings made of an assembly of deposited preformed clusters, which have not lived sufficiently long to rearrange into a stable crystalline state. Despite the absence of complete characterization of the

atomic structure within this pretransition state, it is reasonable to assess that this poorly organized structure has accumulated large strain energy. It is then rather unstable and quite prone to suffer from a mechanically induced collapse. Further insight into the flattening process itself is provided by the layer-by-layer structure revealed in Figure 5b, which is quite characteristic of a lamellar arrangement. Moreover in most cases, we observed that compact features may remain superimposed to a crystalline flat base (see a few examples in Figure 5). This reveals that the flattening transition proceeds from the bottom. Consequently, we can propose that a first crystalline layer takes place on the graphite surface and that upper ones are created sequentially as long as there remains sufficient mass to extend the process.

The cooperative nature of the transition at the level of the whole island raises further questions. It is initiated at given endings but it seems difficult to attribute its propagation over the whole island as due to mechanical waves through the narrow arms of the fractal. As pointed out by Sapoval et al.,[14] the fractal structure close to the center of the islands generally induces a strong confinement of the waves analogous to superlocalization and then damps the propagation. We therefore propose an alternative mechanism. The cooperative nature settles up thanks to the crystallization of a first layer in contact with the graphite surface that spreads rapidly under the whole island, providing the flattening of all endings.

The role of the substrate is certainly weak, since the adhesion energy between the Sb islands and the graphite surface is quite small, as we have noticed during near-field observations, that the islands can easily be moved by the tip. However, it cannot be totally ruled out. The observed limitation of the lateral expansion of the flattened regions (Figure 4b) may be imposed by an elastic deformation of the substrate, induced by the presence of the substrates themselves.

In conclusion, the observed shape generation in islands grown from the deposition of preformed clusters opens new routes for investigating instabilities in nanostructures. These instabilities are induced by inner constraints within the grown nano-objects and not by those applied externally by the substrate. In particular, the unusual flattening 3D to 2D transitions that we have observed in growth processes mimic at the nanoscale the sliding behaviors occurring at macroscopic levels in geological phenomena for instance. Furthermore, the present study leaves many questions open and therefore offers quite stimulating issues for further theoretical description and modeling.

Supporting Information Available: Additional information about imaging techniques recording and interpretation and AFM and STEM images of Sb islands obtained from cluster deposition on HOPG surfaces at room temperature. This material is available free of charge via the Internet at http://pubs.acs.org.

References

(1) Leonard, D.; Krishnamurty, M.; Reaves, C. M.; Denbaars, S. P.: Petroff, P. M. *Appl. Phys. Lett.* **1993**, *63*, 3203−3206.
(2) Marzin, J.-Y.; Gérard, J.-M.; Izraël, A.; Barrier, D.; Bastard, G. *Phys. Rev. Lett.* **1994**, *73*, 716−719.
(3) Bréchignac, C.; Cahuzac, Ph.; Carlier, F.; de Frutos, M. Masson, A. Mory, C.; Colliex, C. Yoon, B. *Phys. Rev. B* **1998**, *57*, R2084−R2087.
(4) Yoon, B.; Akulin, V. M.; Bréchignac, C.; Cahuzac, Ph.; Carlier, F.; Colliex, C.; de Frutos, M.; Masson, A.; Mory, C. *Surf. Sci.* **1999**, *443*, 76−88.
(5) Bardotti, L.; Jensen, P.; Hoareau, A.; Treilleux, M.; Cabaud, B. *Phys. Rev. Lett.* **1995**, *74*, 4694−4697.
(6) Jensen, P. *Rev. Mod. Phys.* **1999**, *71*, 1695.
(7) Stegemann, B.; Ritter, C.; Kaiser, B.; Rademann, K. *J. Phys. Chem B* **2004**, *108*, 14292−14297.
(8) Bréchignac, C.; Cahuzac, Ph.; Carlier, F.; Colliex, C.; Le Roux, J.; Masson, A.; Yoon, B.; Landman U. *Phys. Rev. Lett.* **2002**, *88*, 196103.
(9) Kaiser, B.; Stegemann, B.; Kaukel, H.; Rademann, K. *Surf. Sci.* **2002**, *496*, L18−L32.
(10) Sornette, D. *Critical phenomena in natural sciences, chaos, fractals, self-organization and disorder: concepts and tools*, 2nd ed.; Springer Series in Synergetics; Springer: Heidelberg, 2004.
(11) Bréchignac, C.; Cahuzac, Ph.; Carlier, F.; de Frutos, M.; Leygnier, J.; Roux, J. Ph. *J. Chem. Phys.* **1995**, *102*, 763−769.
(12) Witten, T. A.; Sander, L. M. *Phys. Rev. Lett.* **1981**, *47*, 1400−1403.
(13) Bernhardt, T.; Stegemann, B.; Kaiser, B. Rademann, K. *Angew. Chem., Int. Ed.* **2003**, *42*, 199−202.
(14) Sapoval, B.; Gobron, Th.; Margolina, A. *Phys. Rev. Lett.* **1991**, *67*, 2974−2977.
(15) Irasawa, T.; Uwaha, M.; Saito, Y. *Europhys. Lett.* **1995**, *30*, 139−144.

NL060781N